6th European Conference on Computational Mechanics (ECCM 6)
7th European Conference on Computational Fluid Dynamics (ECFD 7)
1115 June 2018, Glasgow, UK

PARAMETER ESTIMATION IN A DIAGNOSTIC WIND MODEL OVER COMPLEX TERRAIN

G. Montero[1], E. Rodríguez[1], A. Oliver[1] and J. Calvo[2]

[1] SIANI - University of Las Palmas de Gran Canaria, Edificio Polivalente I, Campus Universitario de Tafira, Las Palmas de Gran Canaria, Spain, (gustavo.montero, eduardo.rodriguez, albert.oliver)@ulpgc.es, http://www.dca.iusiani.ulpgc.es/proyecto2015-2017/html/index.html

[2] Agencia Estatal de Meteorología (AEMET), Leonardo Prieto Castro, 8, 28040-Madrid, Spain, j.calvo@aemet.es, www.aemet.es

Key words: Parameter Estimation, Wind Modelling, Roughness Parameters, Memetic Algorithms

Abstract. The aerodynamic roughness length (z_0) and the displacement height (d) are critical for wind modelling based on the log vertical profile. It is well known that the values of these parameters depend on weather conditions and land coverage. Thus, many authors have studied its relationship, providing typical ranges for each land coverage. In this work, a comprehensive literature review is performed to collect the ranges of z_0 and d for each surface type. In particular, we have focused on the coverages present in the Information System of Land Cover of Spain (SIOSE) [1]. Using these ranges, we propose a procedure to construct z_0 and d maps through a downscaling wind model. Results from the HARMONIE-AROME and ECMWF mesoscale numerical weather prediction models are downscaled using a 3D diagnostic wind model with adaptive finite element method [2, 3]. The values of z_0 and d are estimated with a memetic algorithm that combines the Differential Evolution method [4], a rebirth operator and the L-BFGS-B algorithm [5]. So, the root mean square error (RMSE) of the wind model is minimised against the observed wind data. This fast procedure allows updating the roughness parameters for any weather condition. Some numerical experiments are presented to show the performance of this methodology. Although we work with the SIOSE database and the Wind3D model, the method can be used in conjunction with other databases and downscaling models.

1 INTRODUCTION

The influence of aerodynamic parameters in the modelling of wind field in the microscale and mesoscale, specially the wind velocity near the ground, is well known. Therefore, the accuracy of these parameters is critical to simulate the wind field used in wind power plants energy prediction, dispersion of air pollution, and wildland fire spread among others. In this paper we propose a strategy to improve the results of a downscaling wind

model by estimating the values of the roughness length (z_0) and displacement height (d) using Differential Evolution (DE) and a rebirth operator (RO).

A downscaling wind model uses the prediction of a Numerical Weather Prediction (NWP) model as input wind field to compute a new one in a higher resolution mesh that better captures the terrain features. In this paper, the downscaling wind model is Wind3D [3], a diagnostic mass-consistent wind model with an updated atmospheric parameterisation and wind profile proposed in [6, 7, 8], and it is coupled with two different NWP models: specifically the European Centre for Medium-Range Weather Forecasts (ECMWF) model [9] and the HARMONIE-AROME model [10]. In this paper we have used the land cover database of Spain (SIOSE) [1].

The content of the paper is organised as follows. As a first step, we need to know the different land covers of the region that, in this case, are given by the SIOSE database described in Sect. 2. Then, we identify the suitable ranges of z_0 and d for each land cover; these ranges are given in the literature and shown in Sect. 3. For a given region there exists a combination of different land covers, so we need to compute the actual value of each aerodynamic parameter by using the formula presented in Sect. 3 too. Then, with these values and the forecast wind field of the NWP model, we simulate the resulting wind field with the Wind3D model (Sect. 4). The last step of the algorithm is to compute the fitting function (the root square mean error between the predicted and the observed wind in meteorological stations) and generate the next population of the optimisation algorithm (Sect. 5). Numerical experiments in a realistic case in Gran Canaria Island are described in Sect. 6. Finally, the conclusions of this work are summed up in Sect. 7.

2 SIOSE LAND COVER DATABASE

In 1990, the first land cover database encompassing the whole national territory was constructed in Spain on a scale of $1 : 100.000$. It was developed in the framework of the CORINE Land Cover (CLC) European project [11]. After successive updates in 2000, 2006 and 2012, it became Image & CORINE Land Cover. The SIOSE database consists of different basic (40) and compound coverages. A compound coverage is made up of a combination of basic ones. It considers eight general groups of basic coverages (Crops, Grassland, Forest, Scrubs, No Vegetation, Artificial Coverage, Wet Coverage and Water Coverage) that are further refined into forty specific classes of basic coverage; see [12].

3 ROUGHNESS LENGTH AND DISPLACEMENT HEIGHT

To obtain siutable values of z_0 and d, we must define the search space of them. We have carried out a literature review to find the ranges of z_0 and d values showed in Table 1 for each land cover; see [3]. The first and second columns show the SIOSE code and a description for each land coverage. The third and fourth, and the fifth and sixth columns present the nominal value and the range of the parameters z_0 and d, respectively.

The SIOSE project uses a vectorial format, but, for convenience, we will translate it to a raster format. For this, we will define a grid with n_p points and, for each point, we will look for the mean value of basic coverages. Once we have the values of z_0 and d for

Table 1: Nominal values and ranges of z_0 and d for the land cover classes provided by SIOSE.

Code	**Land Cover**	$\boldsymbol{z_0}$ (m)	$\boldsymbol{z_{0min}}$–$\boldsymbol{z_{0max}}$	$\boldsymbol{d}$ (m)	$\boldsymbol{d_{min}}$–$\boldsymbol{d_{max}}$
ACM	Sea Cliffs	0.05	0.05–0.19	57	3.3–85
ACU	Water Courses	0.00025	0.0001–0.01	0	–
AEM	Water body. Reservoirs	0.00025	0.0001–0.005	0	–
AES	Estuaries	0.0002	0.0001–0.01	0	–
ALC	Coastal Lagoons	0.005	0.0001–0.01	0	–
ALG	Water body.				
	Lakes and Lagoons	0.0005	0.0001–0.005	0	–
AMO	Seas and Oceans	0.0002	0.0001–0.03	0	–
ARR	Rocky Outcrops and Rocks	0.005	0.0003–0.18	0.03	0–0.96
CCH	Screes	0.1	0.05–0.15	0.6	0.56–0.66
CLC	Quaternary lava flow	0.0286	0.0013–0.0735	0.15	0–0.4
CNF	Forest. Conifers	1.28	0.25–1.93	13.1	4.87–22
CHA	Herbaceous crops. Rice	0.072	0.001–0.11	0.85	0.1–1.55
CHL	Herbaceous crops.				
	Different from Rice	0.1	0.004–0.74	0.25	0.1–3
EDF	Artificial Coverage.				
	Buildings	1.5	0.7–3.7	14	7–19.73
FDC	Forest. Leafy. Deciduous	1	0.18–1.4	11.8	3–21.6
FDP	Forest. Leafy. Evergreen	0.72	0.6–2.65	9.7	3–31
GNP	No Vegetation.				
	Glaciers and				
	Perpetual Snow	0.001	0.00001–0.012	0.01	0–0.06
HMA	Salt Marshes	0.11	0.0002–0.17	0.6	0–0.93
HPA	Wetlands	0.1	0.005–0.55	0.55	0.03–3
HSA	Continental Salt Mines	0.01	0.0005–0.04	0.05	0–0.22
HSM	Salt Lakes	0.01	0.0005–0.04	0.05	0–0.22
HTU	Peat bogs	0.03	0.0005–0.03	0.16	0–0.16
LAA	Artificial Coverage.				
	Artificial water body	0.0001	0.0001–0.005	0	–
LFC	Woody Crops.				
	Citrus Fruit Trees	0.31	0.03–0.4	3	0–4
LFN	Woody Crops.				
	No Citrus Fruit Trees	0.25	0.03–1	0.92	0–4
LOC	Other Woody Crops	0.0615	0.0369–0.0861	0.33	0.2–0.47
LOL	Olive Groves	0.48	0.25–0.61	2.67	2–3
LVI	Vineyards	0.2	0.08–0.55	0.75	0.31–1.4
MTR	Scrubs	0.16	0.016–1	4.8	0.9–7.1

Table 1: *Continued*

Code	**Land Cover**	$z_0\,(m)$	z_{0min}–z_{0max}	$d\,(m)$	d_{min}–d_{max}
OCT	Artificial Coverage.				
	Other Buildings	0.5	0.06–1	4	2–14
PDA	No Vegetation.				
	Beaches, Dunes and Sandy Areas	0.0003	0.0003–0.06	0	0–0.33
PRD	Crops. Meadows	0.03	0.001–0.1	0.013	0.007–0.035
PST	Grasslands	0.09	0.001–0.15	0.171	0.013–0.66
RMB	No Vegetation. Ravines	0.0012	0.0003–0.005	0.03	0–0.03
SDN	No Vegetation. Bare Soil	0.001	0.0002–0.04	0.03	0–0.22
SNE	Artificial Coverage.				
	Unbuilt Land	0.0003	0.0002–0.04	0	0–0.22
VAP	Artificial Coverage.				
	Road, Parking or Unvegetated				
	Pedestrian Areas	0.03	0.0035–0.5	1	0.02–2.5
ZAU	Artificial Coverage.				
	Artificial Green Area and				
	Urban Trees	0.4	0.03–1.3	3.5	3.5–14
ZEV	Artificial Coverage.				
	Extraction or Waste Areas	0.1	0.0003–0.18	0.16	0–1
ZQM	No Vegetation. Burnt Areas	0.6	0.1–1.1	3.27	0.54–6

each basic coverage, we can compute the specific z_0 and d values at any point using an appropriate weighted mean. This way, the SIOSE database will let us create a matrix with the percentage of the basic coverages at any point. This matrix is defined as follows: let M be an $n_p \times n_b$ matrix, with components $m_{i,j}$, where n_b is the number of basic coverages. For each row i of M, $m_{i,j}$ is the fraction of the basic coverage j at the point n_i ($m_{i,j} < 1$ and $\sum_{j=1}^{n_b} m_{i,j} = 1$). When the ranges of z_0 and d are set for each basic land coverage, we can compute its values at any point of the terrain. Assuming that the values of z_0 and d are a certain mean of the values of the basic coverages z_{0j} and d_j, $j = 1, \ldots, n_b$, we can compute their values at any point. In this case, the formula proposed by [13] was applied. For a coverage i composed by n_b basic canopies with roughness length z_{0j}; $j = 1, \ldots, n_b$ on a fraction m_{ij} of the area, respectively, the effective z_0 is approximated by:

$$z_0 = \prod_{j=1}^{n_b} z_{0j}^{m_{ij}}. \tag{1}$$

Regarding d, it is known that the effective displacement height of a heterogeneous coverage can exceed the mean canopy height significantly. So, we propose to use a weighted

root mean square to obtain a higher mean value than Taylor's one:

$$d = \sqrt{\sum_{j=1}^{n_b} m_{ij} d_j^2}, \tag{2}$$

where d_j and m_{ij} are the displacement height and the fraction of the basic coverage j in the composed one i, respectively. Figures 1(a) and (b) show the resulting composed z_0 and d values in Gran Canaria for the nominal values of basic coverages given in Table 1.

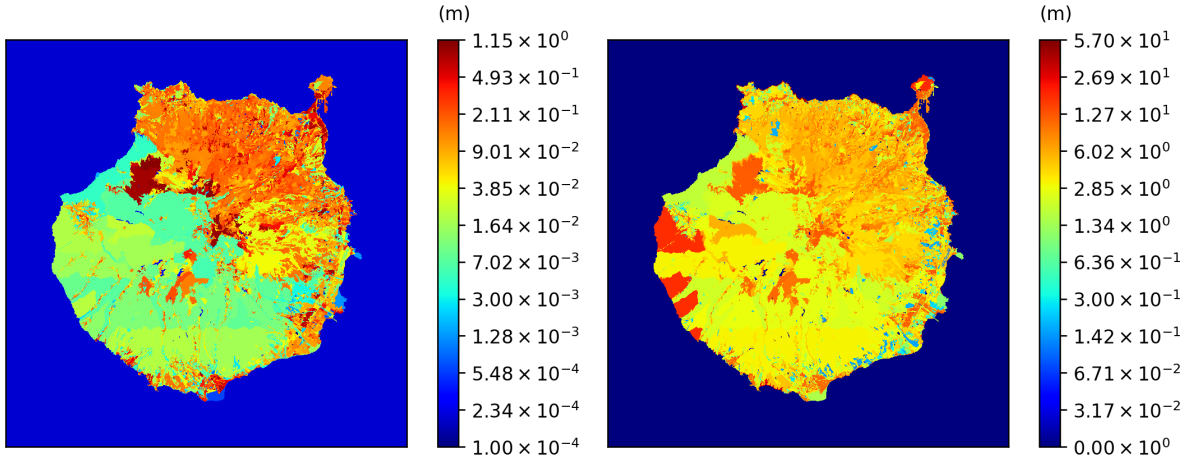

(a) Roughness length (z_0) map (b) Displacement height (d) map

Figure 1: Roughness length and displacement height maps of Gran Canaria island (m) corresponding to the nominal values stated in Table 1 and using the mean values given in equations (1) and (2), respectively.

4 DIAGNOSTIC WIND MODEL

We consider a mass-consistent model [3] to compute a wind field u in a domain Ω with a boundary $\Gamma = \Gamma_a \cup \Gamma_b$, which satisfies the mass continuity equation in Ω, for an incompressible flow, and the impermeability condition on the terrain Γ_a:

$$\nabla \cdot u = 0 \quad \text{in } \Omega, \tag{3a}$$

$$n \cdot u = 0 \quad \text{on } \Gamma_a, \tag{3b}$$

where n is the outward-pointing normal unit vector and Γ_b the free boundary. The model formulates a least-squares problem in the domain Ω to find a wind field $u = (u_x, u_y, u_z)$, such that it is adjusted as much as possible to an interpolated wind field $u_0 = (u_{0x}, u_{0y}, u_{0z})$. The adjusting functional for a field $v = (v_x, v_y, v_z)$ is defined as:

$$e(v) = \frac{1}{2} \int_\Omega (v - u_0)^T P (v - u_0) \, d\Omega, \tag{4}$$

where $(v-u_0)^T$ is the transpose of $(v-u_0)$, P is the 3×3 diagonal transmissivity matrix with $P_{1,1}=P_{2,2}=2\alpha_1^2$ and $P_{3,3}=2\alpha_2^2$, being α_1 and α_2 the Gauss Precision moduli. The Lagrange multiplier technique is used to minimise the functional (4), with the restrictions (3). Considering the Lagrange multiplier λ, the Lagrangian is defined as:

$$L\left(v,\lambda\right)=e\left(v\right)+\int_{\Omega}\lambda\nabla\cdot v\;d\Omega, \tag{5}$$

and the solution u is obtained by finding the saddle point (u,ψ) of the Lagrangian (5). This resulting wind field satisfies the Euler-Lagrange equation:

$$u=u_0+P^{-1}\nabla\psi, \tag{6}$$

where ψ is the Lagrange multiplier. If α_1 and α_2 are constant in Ω, substituting (6) in (3), the problem results in an elliptic PDE in ψ to be solved with FEM:

$$\frac{\partial^2\psi}{\partial x^2}+\frac{\partial^2\psi}{\partial y^2}+\alpha\frac{\partial^2\psi}{\partial z^2}=-2\alpha_1^2\left(\frac{\partial u_{0x}}{\partial x}+\frac{\partial u_{0y}}{\partial y}+\frac{\partial u_{0z}}{\partial z}\right) \qquad \text{in } \Omega, \tag{7a}$$

$$-n\cdot P^{-1}\nabla\psi=n\cdot u_0 \qquad \text{on } \Gamma_a, \tag{7b}$$

$$\psi=0 \qquad \text{on } \Gamma_b, \tag{7c}$$

where $\alpha=\alpha_1/\alpha_2$ is the ratio of the Gauss Precision Moduli.

The interpolated wind field is computed in the whole domain Ω from pointwise wind data. The wind data can come from measurement stations or a numerical weather prediction system. In this work, we will use the HARMONIE-AROME forecast wind field, as proposed by [2]. Using these data, we construct the interpolated wind field, u_0 in two steps: first, a horizontal interpolation and, then, a vertical extrapolation; see [3].

5 PARAMETER ESTIMATION

The results of the mass-consistent model are very sensitive to the values of α, ξ, z_0, and d. Thus, an accurate definition of these parameters is critical to obtain a reliable wind field. We have to estimate a value of α and ξ for the whole domain, and a value of z_0 and d for each land cover class. This means that the number of unknowns depends on the number of different land covers in the region of interest. These parameters are estimated using a memetic method to optimise a fitness function described in this section.

The objective of the optimisation is to find the values of the parameters such that the wind computed with the model is the most similar to a known wind at some control points. The wind values at the control points are given by the HARMONIE-AROME model or measurement stations. The error between the model and the known data is,

$$RMSE=\sqrt{\frac{1}{n_c}\sum_{i=1}^{n_c}(u_{xi}-u_{xi}^c)^2+(u_{yi}-u_{yi}^c)^2+(u_{zi}-u_{zi}^c)^2}, \tag{8}$$

where n_c is the number of control points, (u_{xi},u_{yi},u_{zi}) and $(u_{xi}^c,u_{yi}^c,u_{zi}^c)$ are, respectively, the wind velocity obtained with the mass-consistent model and the known wind at the i^{th}

control point. So, the parameter estimation consists of the minimisation of the RMSE. Note that for each evaluation of the fitness function, the wind model has to be executed.

The optimisation strategy is based on a memetic method composed of three tools: DE [4], a Rebirth Operator (RBO) [14], and the L-BFGS-B algorithm [5]. DE is an evolutionary algorithm that utilises a population composed of a fixed number n_v of D-dimensional parameter vectors $p_{i,g}$ for each generation g; $g = 1, \ldots, n_g$. The initial population, which must cover the parameter searching space, is chosen randomly. The mutation procedure modifies an existing vector by adding to itself a weighted difference between two other vectors. In the crossover step, these mutated vectors are mixed with another target vector to obtain the so-called trial vector. If the trial vector yields a lower fitness function value than the target vector, the target vector is replaced by the trial vector (selection). Each population vector has to serve as target vector at least once, so n_v competitions will take place per generation.

The accuracy of the results obtained using DE may be insufficient. To increase it, we have run n_e DE experiments and have performed a statistic analysis of the results obtained for each one. This analysis will allow us to reduce the search interval. Let $p^j_{i,n_g}(j = 1, \ldots, n_e;\ i = 1, \ldots, n_u)$ be the estimation of the n_u unknown parameters obtained in each of the n_e experiments. We can compute its average $\overline{p}_{i,n_g}$, and standard deviation σ_{i,n_g}. Then, the search interval can be reduced to the confidence interval of each variable, i.e., $\overline{p}_{i,n_g} \pm \frac{\sigma_{i,n_g}}{\sqrt{n_e}} T_{n_e-1,\frac{\tau}{2}}$, where $1-\tau$ is the confidence coefficient and T, the Student's t-distribution. If one extreme of the new interval exceeds the old extreme, the latter is preserved. This allows the rebirth of a new population to restart DE. This procedure may be repeated as many times as required. Note that the n_e DE experiments can be run in parallel. When the last generation of the last reborn population is evaluated, the best parameter vector among all the DE experiments is selected to be the starting point of the L-BFGS-B algorithm. This algorithm is a procedure for solving large non-linear optimisation problems with simple bounds. It is based on the gradient projection method and uses a limited memory BFGS matrix to approximate the Hessian of the fitness function. The results of this final minimisation will be the estimated parameters.

6 NUMERICAL EXPERIMENT

In this section, an experiment is presented. It was an application in an eastern location of Gran Canaria, using the HARMONIE-AROME and ECMWF models and the measurement wind data from the AEMET network of stations. In this experiment, we apply the described methodology to a region of the Gran Canaria island. The downscaling model uses the forecast from HARMONIE-AROME and ECMWF. The memetic algorithm estimates the roughness length and displacement height.

The region of interest is a domain of 12 km × 28.5 km × 3 km located at the East of Gran Canaria. The tetrahedral mesh is adapted to the terrain with additional local refinement around the measurement stations and the shoreline; see a detail of the terrain triangulation in Fig. 2(a). The mesh contains 44 970 tetrahedra and 10 070 nodes. The land coverages are taken from the SIOSE database. Since, in Gran Canaria, the range of variation of

environmental temperature is rather small throughout the year, the land coverages may be considered constant in size and shape. Precisely, in the region of interest, there are 1216 land cover polygons, each with a particular combination of 26 basic coverages.

Table 2: Selected wind episodes in an Eastern region of Gran Canaria during June 2015.

BL stability	**HARMONIE 10 m wind speed (ms^{-1})**	**HARMONIE 10 m wind direction (°)**	**Surf. buoy. flux, B_s (m^2s^{-3})**	**B-V freq., N_{2h-h} (s^{-1})**	**Ratio V_*/W_***
LS	10.18	336.92 – NNW	-1.38×10^{-4}	1.68×10^{-2}	–
NS	6.10	331.46 – NNW	-9.78×10^{-4}	≈ 0	–
TN	7.51	331.82 – NNW	≈ 0	≈ 0	–
CN	8.52	340.72 – NNW	3.68×10^{-3}	1.04×10^{-2}	–
PC	1.59	116.78 – ESE	6.22×10^{-3}	1.54×10^{-2}	0.17
MC	6.87	358.98 – N	3.02×10^{-3}	1.74×10^{-2}	0.76

The roughness parameters depend on wind velocity and stability due to the fact that they characterise the surface that influences the wind speed profile (so-called footprint). This footprint is dependent on stability and height (in general, boundary layer conditions), and so indirectly are the roughness parameters. The stability dependence of the roughness length and displacement height was demonstrated by [15]. For this reason, we have chosen six episodes to carry out the experiment, each one corresponding to a different stability class. Table 2 shows the selected episodes indicating the stability class, the 10 m wind speed and direction, and the values of the B_s, N_{2h-h}, W_*, and V_*. These values are the HARMONIE-AROME predictions for June 2015. The stability class has been defined using the B_s values and N_{2h-h} or the comparison between W_* and V_* values, according to [8]. We want to emphasise that, although we have defined the third episode of Table 2 as Truly Neutral (the only case out of 240 for the whole period), it corresponds to a Conditionally Neutral boundary layer with very small B_s and N_{2h-h}. The same occurs with the Nocturnal Stable case, which may also be considered as a Long-Lived Stable boundary layer with a very small N_{2h-h}. Moreover, the selected PC episode is the only one with ESE wind direction in that month. In the studied period, most episodes were LS (44.58 %), MC (41.25 %), or CN (9.58 %). For each of the six chosen episodes, the memetic algorithm estimates the values of α, and the 26 basic coverages z_0 and d. The searching space for the aerodynamic parameters is the one given in Table 1. Regarding α, its values ranges from 10×10^{-2} to 1 in SBL and from 1 to 5 in CBL.

Wind measures at four stations of the AEMET network are available in the studied region. Their UTM coordinates and heights above sea level are given in Table 3 and shown in Fig. 2(a). Two different experiments have been carried out; one using data from HARMONIE-AROME, and the other using data from ECMWF. Figure 2(a) shows the grid points from both NWP models. The wind velocities are plotted for a particular episode. The interpolated wind field is built from the NWP wind velocities at 10 m.

Table 3: Location in UTM zone 28N coordinates and heights above the sea level of the anemometers used in the numerical application in Gran Canaria Island.

Code	**Name**	$\boldsymbol{x}$ (m)	$\boldsymbol{y}$ (m)	$\boldsymbol{z}$ (m)
C639U	San Bartolomé de Tirajana, El Matorral	455345	3076503	51
C648C	Aguimes	455326	3086484	316
C649I	Gran Canaria, Aeropuerto	461659	3088640	34
C649R	Telde, Melenara	462855	3095805	19

Finally, we estimate the parameters using the memetic algorithm described in Sect. 5. The control points used to compute the RMSE are different for the two experiments. In the case of the HARMONIE-AROME, there are 28 control points: the wind data of four stations and the 24 HARMONIE-AROME 10 m wind located over the sea. In the ECMWF experiment, there are the four stations and two more ECMWF points over the sea; see Fig. 2(a). The results of the experiments are condensed in Table 4 as the RMSE values for the six episodes. These RMSE values are always constructed against the measurement wind data from the meteorological stations. The first three rows correspond to the HARMONIE-AROME experiment, while the last three correspond to the ECMWF experiment. Each group of three rows has to be read the same way: the first row is the RMSE obtained by NWP forecast; the second row is the error obtained by the downscaling model Wind3D using the nominal values from Table 1; i.e. without using the memetic algorithm; and the third row are the errors with the memetic procedure.

Table 4: Experiment results with data from HARMONIE-AROME and ECMWF.

Wind direction	**NNW**	**NNW**	**NNW**	**NNW**	**N**	**N**
Wind speed (ms^{-1})	$\boldsymbol{v > 6}$	$\boldsymbol{v > 6}$	$\boldsymbol{v > 6}$	$\boldsymbol{v > 6}$	$\boldsymbol{v \leq 2}$	$\boldsymbol{v > 6}$
Stability	**LS**	**NS**	**TN**	**CN**	**PC**	**MC**
RMSE(H-A)	8.47	3.12	5.94	7.89	3.29	2.46
RMSE(H-A/W3D) nominal values	4.00	3.47	4.74	6.21	2.55	2.40
RMSE(H-A/W3D) estimated values	2.44	2.59	3.47	4.78	2.27	1.31
RMSE(ECMWF)	7.08	3.88	3.16	6.14	2.97	2.98
RMSE(ECMWF/W3D) nominal values	4.00	3.47	4.74	6.21	2.55	5.90
RMSE(ECMWF/W3D) estimated values	2.56	2.91	3.68	4.79	2.53	2.35

Looking at the results, in the HARMONIE-AROME experiment, there has been an improvement between 16.99 % and 71.19 % comparing the results from the NWP and the wind obtained using the described procedure. In the ECMWF experiment, the improvement is similar to the one obtained in the HARMONIE-AROME experiment, except in the TN episode. In this case, the downscaling model has not been able to improve the ECMWF forecasting. Looking at the differences in RMSE between the downscaling forecast using nominal or estimated values, the necessity of estimating z_0 and d gets clear;

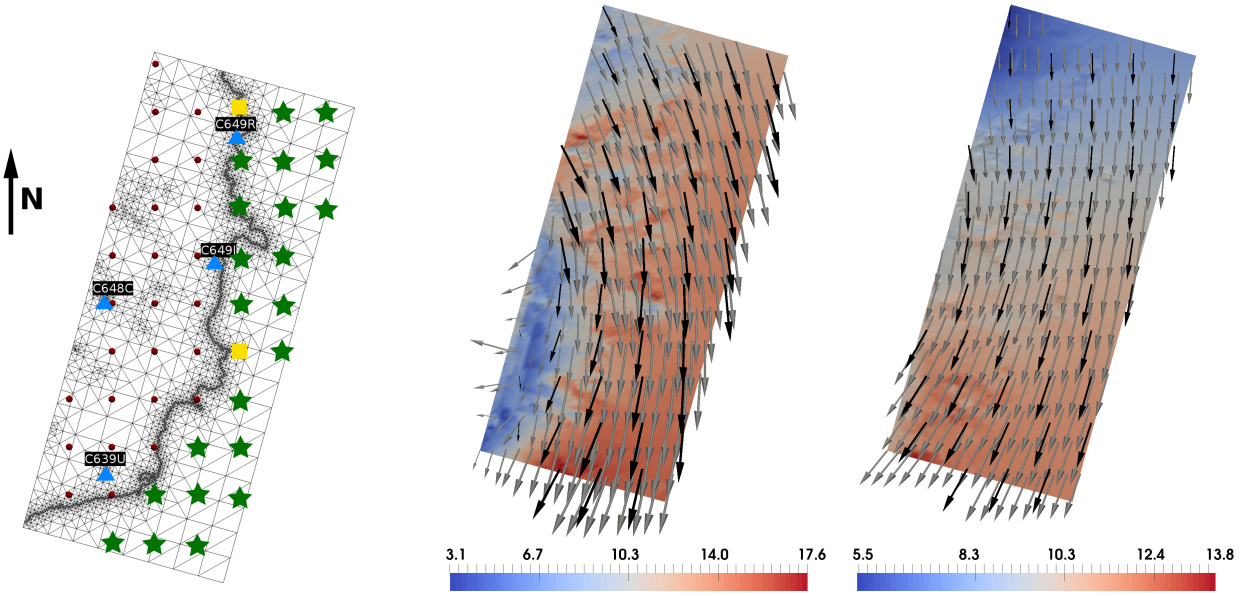

(a) Adaptive mesh (b) Long-Lived Stable (c) Mechanically-Convective Layer

Figure 2: Detail of the adaptive mesh of Gran Canaria Island (a). The symbols indicate the locations of the data falling inside the domain: the triangles represent the measurement stations; the stars, the control points of HARMONIE-AROME only; the squares, the control points of both HARMONIE-AROME and ECMWF; and the circles, the additional grid points of HARMONIE-AROME used in the mass-consistent model. Detail of 10 m wind velocities in the (b) LS and (c) MC cases of Table 2. The colours represent the wind speed obtained by Wind3D. The black vectors are the wind velocities provided by HARMONIE-AROME. The grey vectors are the downscaled wind velocities.

the errors are always smaller for the estimated values. Figure 2 represents the forecast 10 m wind velocities for the LS and MC episodes. The wind field represented is the HARMONIE-AROME forecast and the Wind3D with estimated values results. We observe that the mass-consistent model reproduced the HARMONIE-AROME wind, but providing a more accurate wind in the microscale and improving the predictions in the surroundings of the measurement stations (Table 4).

7 CONCLUSIONS

This paper presents a methodology to improve the downscaling forecasting by estimating the involved parameters. These are the ratio of the Gauss precision moduli α, that appears in the governing equation; a weighting parameter ξ used in the horizontal interpolation of wind velocities; and the roughness length z_0 and the displacement height d of each basic cover class in the logarithmic wind profile. To estimate these parameters, a memetic algorithm, consisting of the DE method and L-BFGS-B algorithm, combined with a rebirth procedure based on Student t-distribution confidence interval, is proposed.

A numerical experiment was carried out on a real case in Gran Canaria Island. In this case, the input values of the model came from two different models: HARMONIE-AROME, and ECMWF; and the control points were some measurement stations and mesoscale model nodes over the sea. Some episodes with different atmospheric conditions have been considered. In all cases, the wind prediction of the diagnostic model with the estimated parameters was closer to the measurement data than the one provided by the mesoscale model. Accordingly, we conclude that the proposed approach, combining parameter estimation and a mass-consistent model, is an efficient tool for NWP downscaling.

ACKNOWLEDGEMENTS

This work has been supported by the Spanish Government, "Secretaría de Estado de Investigación, Desarrollo e Innovación", "Ministerio de Economía y Competitividad", and FEDER, grant contract: CTM2014-55014-C3-1-R.

REFERENCES

[1] National Technique Team SIOSE, *Documento Técnico SIOSE2005 Versión 2.2*. Technical report, D.G. Instituto Geográfico Nacional, Madrid, 2011. In Spanish.

[2] Oliver, A., Rodríguez, E., Escobar, J.M., Montero, G., Hortal, M., Calvo, J., Cascón, J.M. and Montenegro, R., Wind forecasting based on the HARMONIE model and adaptive finite elements. *Pure Appl. Geophys.*, Vol. **172**, pp. 109–120, 2015.

[3] Montero, G., Rodríguez, E., Oliver, A., Calvo, J., Escobar, J.M. and Montenegro, R., Optimisation technique for improving wind downscaling results by estimating roughness parameters. *J. Wind Eng. Ind. Aerod.*, Vol. **174**, pp. 411–423, 2018.

[4] Storn, R. and Price, K., Differential Evolution – A Simple and Efficient Heuristic for Global Optimization over Continuous Spaces. *J. Glob. Optim.*, Vol. **11**, pp. 341–359, 1997.

[5] Byrd, R.H., Lu, P., Nocedal, J. and Zhu, C., A Limited Memory Algorithm for Bound Constrained Optimization. *SIAM J. Sci. Comput.*, Vol. **16**, pp. 1190–1208, 1995.

[6] Zilitinkevich, S.S., Fedorovich, E.E. and Shabalova, M.V., Numerical model of a non-steady atmospheric planetary boundary layer, based on similarity theory. *Bound.-Lay. Meteorol.*, Vol. **59**, pp. 387–411, 1992.

[7] Zilitinkevich, S.S., Johansson, P.E., Mironov, D.V. and Baklanov, A., A similarity-theory model for wind profile and resistance law in stably stratified planetary boundary layers. *J. Wind Eng, Ind. Aerod.*, Vol. **74–76**, pp. 209–218, 1998.

[8] Zilitinkevich, S.S., Tyuryakov, S.A., Troitskaya, Y.I. and Mareev, E.A., Theoretical models of the height of the atmospheric boundary layer and turbulent entrainment at its upper boundary. *Atmospheric and Oceanic Physics*, Vol. **48**(1), pp. 150–160, 2012.

[9] Andersson, E., *User guide to ECMWF forecast products*. Technical report, ECMWF, 2015.

[10] Bengtsson, L., Andrae, U., Aspelien, T., Batrak, Y., Calvo, J., de Rooy, W., et al, The HARMONIE-AROME model configuration in the ALADIN-HIRLAM NWP system. *Monthly Weather Review*, Vol. **145**(5), pp. 1919–1935, 2017.

[11] Bossard, M., Feranec, J. and Otahel, J., *CORINE land cover technical guide Addendum 2000*. Technical report, European Environment Agency; Copenhagen, 2000.

[12] National Technique Team SIOSE, *Manual de Fotointerpretacin SIOSE - Versión 2*. Technical report, D.G. Instituto Geográfico Nacional, Madrid, 2011.

[13] Taylor, P.A., Comments and further analysis on effective roughness lengths for use in numerical three-dimensional models. *Bound.-Lay. Meteorol.*, Vol. **39**, pp. 403–418, 1987.

[14] Greiner, D., Emperador, J.M. and Winter, G., A Limited Memory Algorithm for Bound Constrained Optimization. *Comput. Methods Appl. Mech. Engrg.*, Vol. **193**(33–35), pp. 3711–3743, 2004.

[15] Zilitinkevich, S.S., Mammarella, I., Baklanov, A.A. and Joffre, S.M., The effect of stratification on the aerodynamic roughness length and dis- placement height. *Bound.-Lay. Meteorol.*, Vol. **129**, pp. 179–190, 2008.